

# ExoMol line lists IV: The rotation-vibration spectrum of methane up to 1500 K

Sergei N. Yurchenko and Jonathan Tennyson

*Department of Physics and Astronomy, University College London, London WC1E 6BT, UK*

Accepted XXXX. Received XXXX; in original form XXXX

## ABSTRACT

A new hot line list is calculated for  $^{12}\text{CH}_4$  in its ground electronic state. This line list, called 10to10, contains 9.8 billion transitions and should be complete for temperatures up to 1500 K. It covers the wavelengths longer than  $1\ \mu\text{m}$  and includes all transitions to upper states with energies below  $hc \cdot 18\,000\ \text{cm}^{-1}$  and rotational excitation up to  $J = 39$ . The line list is computed using the eigenvalues and eigenfunctions of  $\text{CH}_4$  obtained by variational solution of the Schrödinger equation for the rotation-vibration motion of nuclei employing program TROVE. An *ab initio* dipole moment surface and a new ‘spectroscopic’ potential energy surface are used. Detailed comparisons with other available sources of methane transitions including HITRAN, experimental compilations and other theoretical line lists show that these sources lack transitions both higher temperatures and near infrared wavelengths. This line list is suitable for modelling atmospheres of cool stars and exoplanets. It is available from the CDS database as well as at [www.exomol.com](http://www.exomol.com).

**Key words:** molecular data; opacity; astronomical data bases: miscellaneous; planets and satellites: atmospheres; stars: low-mass

## 1 INTRODUCTION

Methane plays an important role in atmospheric and astrophysical chemistry. Its rotation-vibration spectrum is of key importance for models of the atmospheres of bodies ranging from Titan to brown dwarfs. Any temperature-dependent model of the methane spectrum requires comprehensive information on the associated transition intensities.

Methane was detected in the exoplanet HD189733b by Swain et al. (2008) and further studied using ground-based observations by Swain et al. (2010). However the abundance of exoplanetary methane has sometimes proved controversial (Stevenson et al. 2010; Beaulieu et al. 2011). On earth methane is an important global warming species (Rhoderick & Dorko 2004) and a biosignature (Sagan et al. 1993); Spectra of hot methane are also required for a variety of

terrestrial applications including the study of combustion (Jourdanneau et al. 2007) and sensing (Wolff et al. 2013). Methane has been detected on Mars (Atreya et al. 2007) although these observations have not always proved repeatable (Krasnopolsky 2012). On earth-like planets outside our solar system, whose spectra of course have yet to be observed, methane has long been thought of as a key potential biosignature (Sagan et al. 1993; Atreya et al. 2007).

Methane is well known in cool carbon stars and brown dwarfs (Bernath 2009); indeed T-dwarfs are often referred to as methane dwarfs (Lucas et al. 2010). However modelling methane in these objects with available laboratory data has often proved difficult (Geballe et al. 1996; Bailey & Kedziora-Chudczer 2012). Similarly hot methane emissions were observed in aftermath of the collision of comet Shoemaker-Levy 9 with Jupiter (Maillard et al. 1995; Dinelli et al. 1997).

Given the importance of methane spectra, a growing number of  $^{12}\text{CH}_4$  rotation-vibration line lists are available. The standard for atmospheric spectroscopy is HITRAN and the recently released 2012 edition (Rothman et al. 2013) contains a thorough update for methane as detailed by Brown et al. (2013). However, HITRAN is designed for work at Earth atmosphere temperatures and its companion, high-temperature database HITEMP (Rothman et al. 2010) does not include methane. Other sources include a high temperature line list computed by Warmbier et al. (2009), the MeCaSDa spectroscopic database containing largely empirical line list (Ba et al. 2013) and a partial experimental line list WKMC constructed by Campargue et al. (2013). Finally high-temperature experimental line lists are available due to Nassar & Bernath (2003), Thiévin et al. (2008), and Hargreaves et al. (2012). Measured methane cross sections are also provided in the PNNL database (Sharpe et al. 2004). As discussed below, none of these compilations are complete at the elevated temperatures considered in this work.

Recently we (Tennyson & Yurchenko 2012) started the ExoMol project which aims to generate a comprehensive library of line list for all molecules likely to be important for modelling atmospheres of exoplanets and cool stars. Here we employ the variational program TROVE (Yurchenko et al. 2007) to construct a synthetic line list for  $^{12}\text{CH}_4$  in its ground electronic state. To this end the Schrödinger equation for the rotation-vibration motion of nuclei is solved to obtain eigenvalues (ro-vibrational energies) and eigenfunctions (nuclear motion wavefunctions). The latter are necessary for ro-vibrational averaging of the dipole moment of the molecule and thus to compute the transitional probabilities, usually expressed in terms of the Einstein coefficients or line strengths. Such calculations are based on the use of a potential energy surface (PES) and dipole moment surfaces (DMSs).

There have been many quantum-chemical studies of methane. We will concentrate on those aimed at producing comprehensive rotation-vibration line lists. Oyanagi et al. (2006) presented *ab initio* PES calculations based at the CCSD(T)/cc-pVTZ and MP2/cc-pVTZ level of theory. Warmbier et al. (2009) used RCCSD(T)/aug-cc-pVTZ theory to compute an hot line list

containing 1.4 millions. Nikitin et al. (2011) constructed a PES which they showed to provide accurate (within  $1 \text{ cm}^{-1}$ ) vibrational energies of  $\text{CH}_4$ . Nikitin et al. (2013) recently presented new *ab initio*, methane DMSs based on the CCSD(T)/cc-pCVQZ level of theory. Rey et al. (2013a,b) employed these PES and DMSs to simulate the room temperature infrared (IR) absorption spectrum of  $\text{CH}_4$ . Comparison with laboratory experiments showed that their predicted intensities agreed well indicating the high-quality of the underlying *ab initio* DMSs. Other recent studies on methane include those by Schwenke & Partridge (2001) and Schwenke (2002), Wang & Carrington (2013) and Mielke et al. (2013).

In this work we present a new ‘spectroscopic’ PES obtained by fitting an *ab initio* PES from Yurchenko et al. (2013) to the experimental energies of  $\text{CH}_4$  with  $J = 0, 1, 2, 3, 4$ . The *ab initio* dipole moment surface (DMS) of Yurchenko et al. (2013), obtained at the CCSD(T)/aug-cc-pVTZ level of theory, is used to compute the line strengths.

The paper is structured as follows. The following section introduces the PES and DMSs, as well as the quantum number scheme used to label the ro-vibrational states of  $\text{CH}_4$  (also discussed in detail in the appendix). Section 3 describes the variational procedure used to solve the Schrödinger equation. The intensity calculations and the line list generated are detailed in Section 4. The evaluation of the new line list and comparisons against different empirical and theoretical line lists are given in Section 6. Some conclusions are offered in Section 7.

## 2 BACKGROUND TO THE CALCULATION

In the following  $\text{CH}_4$  and methane will refer to the main isotopologue  $^{12}\text{CH}_4$  of methane unless specified.

Methane is a symmetric five atomic molecule characterised by nine vibrational degrees of freedom with a vanishing permanent dipole moment. It is a very high symmetry molecule of the  $\mathcal{T}_d(\text{M})$  symmetry group containing a number of degenerate modes. As discussed in our recent work on ammonia (Down et al. 2013), this situation means that some care has to be taken in selecting an appropriate set of quantum numbers. Below we specify our chosen quantum numbers for  $\text{CH}_4$ ; reasons for this choice are given in the appendix.

The symmetry properties of methane spectra have been carefully considered by Hougen (2001) and we used this work as our starting point. Using the Molecular Symmetry group (Bunker & Jensen 2004) the total ro-vibrational states of  $\text{CH}_4$  have total symmetry,  $\Gamma_{\text{tot}}$ , either  $A_1$ ,  $A_2$ ,  $E$ ,  $F_1$ , or  $F_2$ . Considering the H nuclear spin, the nuclear statistical weight,  $g_{\text{ns}}$ , takes the value 5, 5, 2, 3, and 3 for each symmetry respectively. The electric dipole transitions obey the following symmetry-determined selection rules:

$$A_1 \leftrightarrow A_2, E \leftrightarrow E, F_1 \leftrightarrow F_2 \quad (1)$$

**Table 1.**

Mode	Symmetry	Type
1	$A_1$	symmetric stretch
2	$E$	asymmetric bend
3	$F_1$	asymmetric stretch
4	$F_2$	asymmetric bend

**Table 2.** The classification of the multiplicity index  $M_i$  ( $i = 3, 4$ ,  $M_i \leq L_i$ ) by symmetry ( $n = 1, 2, 3 \dots$ )

Symmetry	M
$A_1$	$0 + 12\ n$
$A_2$	$6 + 12\ n$
$E$	$2 + 6\ n$
$F_1$	$3 + 4\ n$
$F_2$	$1 + 4\ n$

with the standard rotational angular momentum,  $\mathbf{J}$ , selection rules:

$$J \leftrightarrow J \pm 1, J' + J'' \neq 0. \quad (2)$$

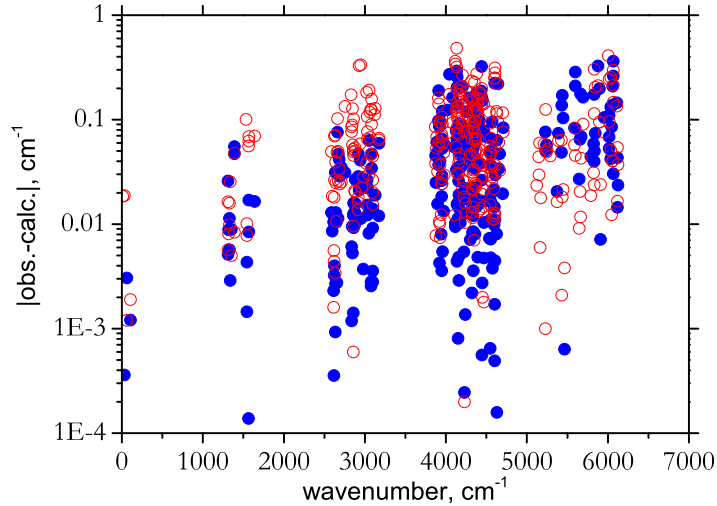
Our set of quantum numbers consists of the following 15 labels:

$$\text{QN} = \Gamma_{\text{tot}}, J, K, \Gamma_{\text{rot}}, n_1, n_2, L_2, n_3, L_3, M_3, n_4, L_4, M_4, \Gamma_{\text{vib}}, N_{J, \Gamma_{\text{tot}}}, \quad (3)$$

where  $\Gamma_{\text{rot}}$  and  $\Gamma_{\text{vib}}$  are the symmetries of the rotational and vibrational wavefunction respectively,  $K = 0, \dots, J - 1$ ,  $J$  is the absolute value of the projection of the rotational angular momentum of  $J$  onto the body-fixed  $z$  axis, and  $n_1, n_2, L_2, n_3, L_3, M_3, n_4, L_4, M_4$  are the normal mode vibrational quantum numbers (see the mode designation in Table 1). We follow Down et al. (2013) and use the only the absolute values of the vibrational angular momentum quantum numbers  $L_i = n_i, n_i - 2, \dots, 0(1)$ .  $M_i \leq L_i$  is a multiplicity index used to count states within a given  $n_i, L_i$  set (see Boudon et al. (2006)) and indicate the symmetry according to Table 2. Finally as it is often not possible to uniquely define  $\text{CH}_4$  quantum numbers, a counting number  $N_{J, \Gamma_{\text{tot}}}$  is also included. This number runs over states of a given total symmetry and  $J$ .

To calculate the ro-vibrational energies in the Born-Oppenheimer approximations, a PES is required. In this work we use a new ‘spectroscopic’ PES obtained by refining an *ab initio* PES through fits to experimental ro-vibrational energies. To this end a set of experimental term values with  $J \leq 4$  was selected ranging up to  $6100\text{ cm}^{-1}$  derived from frequencies collected in the HITRAN 2008 database (Rothman et al. 2009). We recently produced a ‘spectroscopic’  $\text{CH}_4$  PES using a similar procedure by fitting an *ab initio* CCSD(T)-F12/aug-cc-pVQZ PES to the same set of experimentally derived energies (Yurchenko et al. 2013). Here the ‘spectroscopic’ PES of Yurchenko et al. (2013) was further refined. This was necessary because our refinement procedure, and therefore the resulting PES, is sensitive to the size of the basis set used in the variational calculations. The basis set employed here differs from that used by Yurchenko et al. (2013), see below for more details. The resulting PES is given as Supplementary Material to this paper in the form of a Fortran 95 program. It should be noted, however, that this PES has an ‘effective’ character and guarantees to give accurate results only in conjunction with the

**Figure 1.** Residuals of CH<sub>4</sub> experimentally-determined and calculated energy term values. Calculated using the refined PES before the shift of the vibrational band centers (red empty circles) and after (blue filled circles), see text.



same method and basis set used to produce it with. This obvious disadvantage is a result of the non-converged basis set used in TROVE, as well as the approximate character of the kinetic and potential energy expansions employed.

The fitting set of our ‘experimentally-derived’ term values (cm<sup>-1</sup>) was built from combination differences arising from the transition wavenumbers collected in HITRAN 2008. It should be noted that only a few of the term values were supported by more than one transition.

In our procedure, as described in detail by Yurchenko et al. (2011b), the refined PES is formulated as a correction to the original PES:

$$V = V_0 + \Delta V, \quad (4)$$

where both  $V_0$  and  $\Delta V$  are presented as expansion in terms of the internal coordinate displacements. At the first stage, the Schrödinger equations are solved for the initial potential  $V_0$  to obtain the eigenfunctions  $\Psi_{J,\lambda}^{(0)}$  for a set of the rotational quantum numbers  $J$ . These eigenfunctions are then used as basis functions for solving the Schrödinger equations with the probe PES  $V$  during the fitting procedure. In this way only the matrix elements  $\langle \Psi_{J,\lambda} | \Delta V | \Psi_{J,\lambda'} \rangle$  are required when solving the corresponding Schrödinger equations variationally.

The accuracy achieved in this fit is illustrated in Fig. 1, where the absolute values of the obs.-calc. residuals (cm<sup>-1</sup>) are shown. The total root mean square (rms) error for 317 term values used is 0.11 cm<sup>-1</sup> with the major data points distributed between 0.01 and 0.1 cm<sup>-1</sup>. It should be noted however that some of the transitions present in HITRAN 2008 (especially above 5000 cm<sup>-1</sup>) appeared to be relatively large outliers and therefore could not be included into our fitting set. This may indicate problems with our PES for the vibrational modes not properly sampled by our fitting set and/or assignment problems in HITRAN 2008.

### 3 VARIATIONAL CALCULATIONS

The high symmetry of methane meant that a specially adapted version of TROVE had to be developed, details of which are given by Yurchenko et al. (2013). In TROVE the basis set is built using the polyad number, which for  $\text{CH}_4$  is given by

$$P = 2(v_1 + v_2 + v_3 + v_4) + v_5 + v_6 + v_7 + v_8 + v_9, \quad (5)$$

where  $v_i$  is a vibrational quantum number associated with the one-dimensional primitive basis function  $\phi_{v_i}(\xi_i^\ell)$  ( $i = 1, 2, 3, \dots, 9$ ) and  $\xi_i^\ell$  is an internal linearized coordinate, see below. In the conventional normal mode representation this condition corresponds to

$$P = 2(n_1 + n_3) + n_2 + n_4. \quad (6)$$

The stretching basis functions  $\phi_{v_i}(\xi_i^\ell)$  ( $i = 1, 2, 3, 4$ ) were obtained by numerically solving a reduced, one-dimensional Hamiltonian problem using the Numerov-Cooley method. Harmonic oscillators are used for the bending basis functions  $i = 5, 6, 7, 8, 9$ . The basis set used was constructed from two major contributions, (i) all basis functions with the primitive quantum numbers satisfying  $P \leq 10$  and (ii) stretching functions ranging up to  $P = 20$  but with some high  $P$ -polyad ( $P \geq 17$ ) stretching contributions that couple all modes together removed. This scheme is designed to reduce the basis set to the manageable size and at the same time to retain stretching basis functions with higher excitations than bending, giving preference to less-mixed modes. Our underlying assumption for this is that the stretching excitations carry the strongest transitions.

Following Yurchenko et al. (2013), the final contracted basis functions were obtained employing the  $J = 0$  representation. In this representation the  $J = 0$  (vibrational) eigenfunctions are used together with symmetrised rigid rotor functions to construct the basis set functions for  $J > 0$ . For each  $J$  value, five symmetrised Hamiltonian matrices employing the  $J = 0$  contraction scheme are computed and then diagonalized. In order to improve the prediction property of the refined potential of  $\text{CH}_4$  (see Fig. 1) further, artificial band centre shifts were added to the  $J = 0$  energies following the empirical basis set correction scheme (EBSC) (Yurchenko et al. 2009). The result of the improvement can be seen in Fig. 1 as well.

In the TROVE approach the Hamiltonian operator is represented as an expansion around a reference geometry taken here at the molecular equilibrium. The kinetic energy operator is expanded in terms of the nine coordinates  $\xi_i^\ell$ , which are linearized versions of the internal coordinates  $\xi_i$  ( $i = 1, \dots, 9$ ), see (Yurchenko et al. 2013); the potential energy function is expanded in terms of  $1 - \exp(-a\xi_i^\ell)$  ( $i = 1, 2, 3, 4$ ) for the four stretching and  $\xi_j^\ell$  ( $j = 5, 6, 7, 8, 9$ ) for the five bending modes. The latter expansions were applied to the refined PES introduced above. The kinetic and potential energy parts were truncated at sixth- and eighth-order, respectively.

The dimensions of the  $J = 0$  basis sets used are 837, 585, 1418, 1916 and 2163 for the  $A_1$ ,  $A_2$ ,  $E$ ,  $F_1$ , and  $F_2$  symmetries, respectively. The (symmetrically adapted) ro-vibrational basis functions are represented by the (symmetrically reduced) direct product of  $(2J + 1)$  rigid



rotor wavefunctions and the  $J = 0$  eigenfunctions. The size of the ro-vibrational basis set scales linearly with  $J$  as illustrated in Fig. 2, where the size of the  $F_{1x}$  matrix is shown for  $J = 0 \dots 39$ . The largest matrix to be diagonalized ( $F_{1x}$ ,  $J = 39$ ) has  $163\,034 \times 163\,034$  elements. The dimension of the matrices of different symmetries scale approximately in the ratio 1:1:2:3:3 for the  $A_1$ ,  $A_2$ ,  $E$ ,  $F_1$ ,  $F_2$  symmetries, respectively.

LAPACK routine DSYEV and ScaLapack routine PDSYEVD, as implemented in the Intel MKL library, were used to diagonalize the Hamiltonian matrices. The MPI version of LAPACK eigensolver PDSYEVD was used for large matrices with  $J \geq 24$ . All eigen-roots were found in the direct diagonalizations but only eigenvectors below the energy threshold of  $hc \cdot 18\,000 \text{ cm}^{-1}$  were stored and used in the line list production to reduce the calculations and storage. Fig. 3 gives the total number of energy levels and the number of transitions generated from these energy levels as a function of  $J$ , summed over all five symmetries. The linear dependence on  $J$  at lower values is capped at  $J = 21 - 22$  by the energy threshold. At about  $J = 50$  all energy levels of  $\text{CH}_4$  are above  $18\,000 \text{ cm}^{-1}$ . The total number of energy levels subject to the thresholds  $E_{\text{max}} = 18\,000 \text{ cm}^{-1}$  and  $J_{\text{max}} = 39$  is 6 603 166.

#### 4 LINE LIST CALCULATIONS

A spectroscopic line list is a catalogue of transitions containing transition frequencies (or wavenumbers  $\tilde{\nu}_{\text{if}}$ ) and transition line strengths (or Einstein A coefficients  $A_{\text{if}}$ ) between a well-chosen set of initial,  $i$ , and final,  $f$ , states. A line list also necessarily includes the total state degeneracy as well as the lower state energy to allow simulation of absorption or emission spectra at different temperatures. It is also common to include the quantum numbers specifying states involved in each transitions. For more details see (Tennyson 2012; Tennyson et al. 2013).

The goal of this work is a comprehensive line list for  $\text{CH}_4$  covering the wavenumber range up to  $12\,000 \text{ cm}^{-1}$  and applicable for temperatures up to  $T = 1\,500 \text{ K}$ . To be complete at  $T = 1\,500 \text{ K}$ , we estimated that the population is negligible for energies above  $8\,000 \text{ cm}^{-1}$ . This defines our maximal value for lower state energy. We find that at  $J = 40$  all energy term values are above  $8\,000 \text{ cm}^{-1}$ . The lower state energy threshold of  $hc \cdot 8\,000 \text{ cm}^{-1}$  combined with the wavenumber range  $10\,000 \text{ cm}^{-1}$  defines the energy threshold for the upper state to be  $hc \cdot 18\,000 \text{ cm}^{-1}$ , which is also the maximal energy of  $\text{CH}_4$  included in the final line list. That is, the thresholds for the energy and eigenvectors are  $J_{\text{max}} = 39$ ,  $E''_{\text{max}} = hc \cdot 8\,000 \text{ cm}^{-1}$ ,  $E'_{\text{max}} = hc \cdot 18\,000 \text{ cm}^{-1}$ . For the transition calculations we choose an extended wavenumber range up to  $\tilde{\nu}_{\text{max}} = 12\,000 \text{ cm}^{-1}$ , however the maximal temperature is applicable for the transitions up to  $10\,000 \text{ cm}^{-1}$  (wavelengths longwards of  $1 \mu\text{m}$ ) only.

For the total number of levels considered, 6 603 166, the total number of transitions computed is 9 819 605 160, i.e. almost  $10^{10}$ , which is why we call the line list ‘10to10’. Obviously not all these transitions are important at all temperature. However, to demonstrate that a large

number of transitions do matter at elevated temperatures, Fig. 4 shows the density of lines per an absorption intensity  $I_{\text{if}} = A \times 10^x$  unit for different temperatures covering the whole wavenumber range  $0 \dots 12\,000 \text{ cm}^{-1}$ . The slightly deformed Gaussian-like distributions peak at  $x = -39, -33, -32, -30$ , and  $-29$  for  $T = 297, 600, 1000$ , and  $1500 \text{ K}$ , respectively, with long, very small tails spreading up to  $x = -18$  which are not visible at this scale. 98 % of the  $T = 296 \text{ K}$  lines we compute have intensities smaller than  $10^{-32} \text{ cm/molecule}$  and barely contribute to the total opacity at room temperature, and thus can be safely ignored. Conversely at  $T = 1500 \text{ K}$ , where the absorption lines peak at  $I_{\text{if}} 10^{-29} \text{ cm/molecule}$ , most of the hot lines (98 %) appear to be stronger than  $10^{-32} \text{ cm/molecule}$ . Many of these lines also overlap each other, due to the very high density of states, which is not reflected on this figure. In order to bring the line list to a more manageable size, we could apply an intensity cutoff and compiled a reduced version of the line list which gives absorption intensities higher than a certain threshold, say  $10^{-27} \text{ cm/molecule}$ . It is known however that even weaker lines may play important role for non-LTE environments (Dello Russo et al. 2004), which is the reason for keeping even extremely weak absorption transitions in 10to10. In fact there are other, better ways of making this manageable such as cross sections (Hill et al. 2013) or  $k$ -coefficients (Irwin et al. 1996).

Wenger et al. (2008b) calculated the partition function for methane for temperatures up to  $3000 \text{ K}$  by using all states up to the dissociation, whose energies were modelled using different levels of approximations. Figure 7 (upper display) compares this partition function with our values obtained by (a) summing all energies from the 10to10 line list ( $Q^{(18\,000)}$ ) and (b) summing all energies below our lower cut-off of  $8000 \text{ cm}^{-1}$  ( $Q^{(8\,000)}$ ). This latter value is useful as it allows to estimate the completeness of the 10to10 line list as a function of temperature. To quantify this effect the lower display of Fig. 7 also shows the ratio of the two partition functions,  $Q^{(8\,000)}$  and  $Q^{(18\,000)}$ . As discussed above, our set of energies are the subject of the threshold of  $hc \cdot 18\,000 \text{ cm}^{-1}$ , which effects the accuracy of our partition function at higher temperature. At  $1\,000 \text{ K}$ , 10to10 appears to be complete but by  $1\,500 \text{ K}$  the  $8\,000 \text{ cm}^{-1}$  threshold leads to up to 15 % under-sampling which increases rapidly with temperature. Similar behaviour can be expected for the absorption intensities when modelled at  $1\,500 \text{ K}$  and higher temperatures.

## 5 THE FORMAT OF THE LINE LIST

We adopt the ExoMol format (Tennyson et al. 2013) for the 10to10 line list. In this format the line list consists of two files: (i) an Energy file containing all information necessary to describe a given energy level including, most importantly, the lower state energies and the total degeneracies; (ii) a Transition file, where the Einstein coefficients for all transitions are specified. In the Energy file each energy level is numbered from 1 to 6 603 166, sorted by  $J$  (from 0 to 39), symmetry ( $A_1, A_2, E, F_1$ , and  $F_2$ ), and energy. The counting number  $i$ , which is the same as the row number, is a unique tag characterizing a given level. The counting number is then



**Figure 2.** Size of the  $F_1$ -symmetry Hamiltonian matrix and the number of eigenvalues below  $18000 \text{ cm}^{-1}$  for each  $J$ .

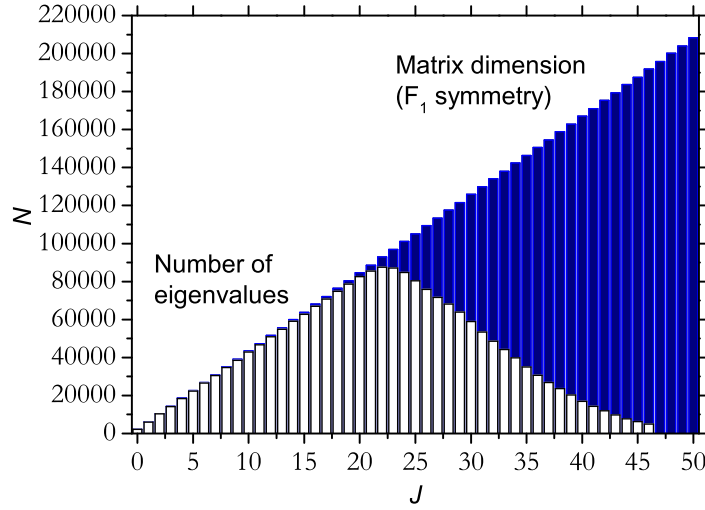
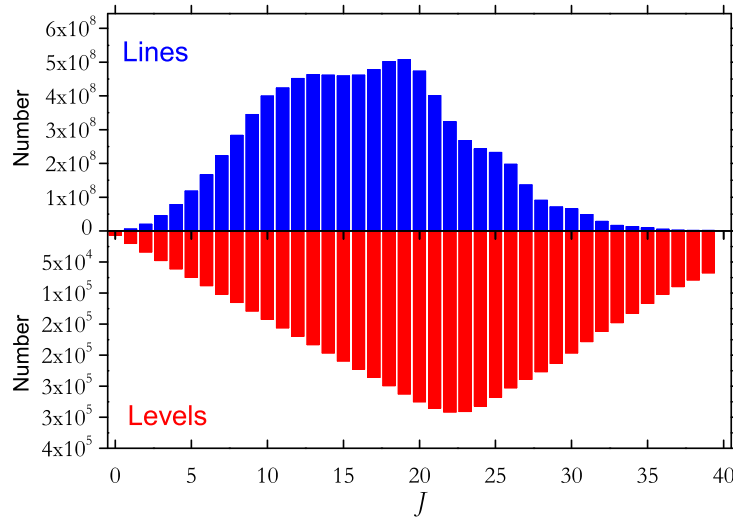


**Figure 3.** Number of energy levels and lines in the 10to10 line list per the rotational quantum number,  $J$ .



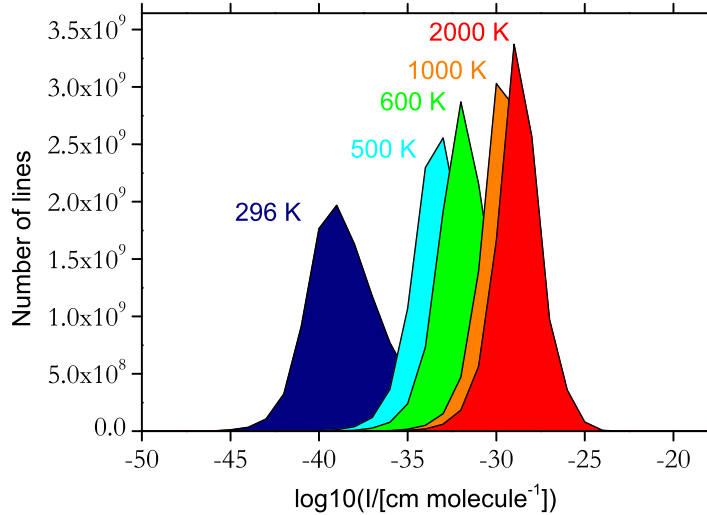
followed by the lower state term value ( $\text{cm}^{-1}$ ) and the total statistical weights  $g_i$ , which for  $\text{CH}_4$  in its ground ( $^1\Sigma$ ) electronic state disregarding the hyperfine splitting, is given by

$$g_i = (2J_i + 1)g_{\text{ns}}^{(i)}. \quad (7)$$

Each energy record also includes the ‘good quantum numbers’  $J$  and  $\Gamma_{\text{tot}}$  (the total symmetry), as well as other quantum numbers from Eq. (3). An extract from the Energy file is given in Table 3.

The Transition file lists the electric dipole transition probabilities in the form the Einstein  $A$  coefficient  $A_{\text{if}}$  in  $\text{s}^{-1}$  for each transition  $i \rightarrow f$  complemented by the  $i$  and  $f$  tags identifying the states in the Energy file, for the lower (initial) and upper (final) states, respectively. For

**Figure 4.** Number of intense lines as a function of intensity for different temperatures. The  $x$ -axis gives the log of the intensity in cm/molecule, while the  $y$ -axis represents the number of transitions per each  $10^x$  cm/molecule bin.



the convenience the Transition file is split into  $100 \text{ cm}^{-1}$  wavenumber pieces (121 files). An extract from one of the Transition files is given in Table 4. According to the ExoMol naming convention, the Energy file is called 10to10.states, while the Transition files are called 10to10-*nnnn*.transitions, where *nnnn* indicates the wavenumber region presented.

The ExoMol website also provides alternative tools allowing the user to convert the line list into different representations, which currently include HITRAN format (Rothman et al. 2013) and the cross-sections, see Hill et al. (2013). We also provide a spectrum program to simulate absorption and emission spectra using the 10to10 line list, in the form of the ‘stick’ spectrum as well as of cross-sections (with different broadenings). The full line list can be also downloaded from the Strasbourg Data Centre (SDC), via <ftp://cdsarc.u-strasbg.fr/pub/cats/J/MNRAS/>, or <http://cdsarc.u-strasbg.fr/viz-bin/qcat?J/MNRAS/>.

## 6 ANALYSIS

In this section we compare the  $^{12}\text{CH}_4$  spectra generated using the 10to10 line list with data available from other sources.

### 6.1 HITRAN

The latest (2012) update of HITRAN contains 336 830 lines of  $^{12}\text{CH}_4$  (Rothman et al. 2013). Figure 5 compares a  $T = 296 \text{ K}$  HITRAN spectrum for  $^{12}\text{CH}_4$  with the spectrum generated from 10to10 at the same temperature. The 10to10 spectral lines are given as sticks with the intensity (cm/molecule) represented by their height. In order to simplify the plot of the 10to10 spectra, only the strongest lines within each 0.01 bin are shown. The HITRAN 2012 data are

**Table 3.** Extract from the 10to10 Energy file.

1	2	3	4	5	6	7	8	9	10	11	12	13	14	15	16	17	18	19	20	21	22	23	24	25	26	27	28	29	30	
$N$	$\tilde{E}$	$g_{\text{tot}}$	$J$	$\Gamma_{\text{tot}}$	$n_1$	$n_2$	$L_2$	$n_3$	$L_3$	$M_3$	$n_4$	$L_4$	$M_4$	$\Gamma_{\text{vib}}$	$J$	$K$	$\tau_{\text{rot}}$	$\Gamma_{\text{rot}}$	$N_{J,\Gamma}$	$ C_i ^2$	$v_1$	$v_2$	$v_3$	$v_4$	$v_5$	$v_6$	$v_7$	$v_8$	$v_9$	
8836	1311.457042	15	1	2	0	0	0	0	0	0	1	1	1	5	1	1	1	4	1	1.00	0	0	0	0	0	0	0	1	0	0
8837	2632.988747	15	1	2	0	0	0	0	0	0	2	2	1	5	1	1	1	4	2	1.00	0	0	0	0	0	0	0	0	1	1
8838	2847.722094	15	1	2	0	1	1	0	0	0	1	1	1	5	1	1	1	4	3	1.00	0	0	0	0	0	1	0	1	0	0
8839	3028.725668	15	1	2	0	0	0	1	1	1	0	0	0	5	1	1	1	4	4	1.00	0	1	0	0	0	0	0	0	0	0
8840	3871.607969	15	1	2	0	0	0	0	0	0	3	1	1	5	1	1	1	4	5	1.00	0	0	0	0	0	0	0	3	0	0
8841	3955.888843	15	1	2	0	0	0	0	0	0	3	3	1	5	1	1	1	4	6	1.00	0	0	0	0	0	0	0	1	2	0
8842	4148.535610	15	1	2	0	1	1	0	0	0	2	2	1	5	1	1	1	4	7	1.00	0	0	0	0	0	1	0	0	1	1
8843	4223.887822	15	1	2	1	0	0	0	0	0	1	1	1	5	1	1	1	4	8	1.00	0	0	1	0	0	0	0	1	0	0
8844	4333.813607	15	1	2	0	0	0	1	1	1	1	1	1	5	1	1	1	4	9	1.00	0	1	0	0	0	0	0	1	0	0
8845	4353.438372	15	1	2	0	2	0	0	0	0	1	1	1	5	1	1	1	4	10	0.97	0	0	0	0	0	2	0	1	0	0
8846	4389.406791	15	1	2	0	2	2	0	0	0	0	1	1	5	1	1	1	4	11	0.97	0	0	0	0	0	0	2	1	0	0
8847	4555.544940	15	1	2	0	1	1	1	1	1	0	0	0	5	1	1	1	4	12	1.00	0	1	0	0	0	1	0	0	0	0
8848	5158.823917	15	1	2	0	0	0	0	0	0	4	2	1	5	1	1	1	4	13	1.00	0	0	0	0	0	0	0	0	1	3
8849	5199.314103	15	1	2	0	0	0	0	0	0	4	4	1	5	1	1	1	4	14	1.00	0	0	0	0	0	0	0	2	1	1
8850	5387.416906	15	1	2	0	1	1	0	0	0	3	1	1	5	1	1	1	4	15	0.99	0	0	0	0	0	1	0	3	0	0
8851	5419.899376	15	1	2	0	1	1	0	0	0	3	3	3	5	1	1	1	4	16	0.98	0	0	0	0	0	1	0	0	2	1
8852	5467.412035	15	1	2	0	1	1	0	0	0	3	3	1	5	1	1	1	4	17	0.98	0	0	0	0	0	1	0	1	2	0
8853	5541.185628	15	1	2	1	0	0	0	0	0	2	2	1	5	1	1	1	4	18	1.00	0	0	1	0	0	0	0	0	1	1
8854	5596.854392	15	1	2	0	0	0	1	1	1	2	0	0	5	1	1	1	4	19	0.99	0	1	0	0	0	0	0	0	2	0
8855	5617.895727	15	1	2	0	0	0	1	1	1	2	2	2	5	1	1	1	4	20	0.95	0	1	0	0	0	0	0	0	0	2
8856	5650.480713	15	1	2	0	2	0	0	0	0	2	2	1	5	1	1	1	4	21	0.86	0	0	0	0	2	0	0	0	1	1
8857	5659.593538	15	1	2	0	0	0	1	1	1	2	2	1	5	1	1	1	4	22	0.85	0	1	0	0	0	0	0	0	1	1
8858	5683.390696	15	1	2	0	2	0	0	0	0	2	2	1	5	1	1	1	4	23	0.96	0	0	0	0	2	0	0	0	1	1
8859	5747.346056	15	1	2	1	1	1	0	0	0	1	1	1	5	1	1	1	4	24	1.00	0	0	1	0	1	0	1	0	1	0
8860	5829.908396	15	1	2	0	1	1	1	1	1	1	1	1	5	1	1	1	4	25	1.00	0	1	0	0	0	1	0	1	0	0
8861	5852.531380	15	1	2	1	0	0	1	1	1	0	0	0	5	1	1	1	4	26	0.95	0	0	2	0	0	0	0	0	0	0
8862	5862.518649	15	1	2	0	1	1	1	1	1	1	1	1	5	1	1	1	4	27	0.95	0	1	0	0	1	0	1	0	1	0
8863	5876.015235	15	1	2	0	3	1	0	0	0	1	1	1	5	1	1	1	4	28	0.92	0	0	0	0	3	0	1	0	0	0
8864	5901.578781	15	1	2	0	3	3	0	0	0	1	1	1	5	1	1	1	4	29	0.92	0	0	0	0	1	2	1	0	0	0
8865	6015.774283	15	1	2	0	0	0	2	2	1	0	0	0	5	1	1	1	4	30	1.00	1	1	0	0	0	0	0	0	0	0
8866	6064.380191	15	1	2	0	2	0	1	1	1	0	0	0	5	1	1	1	4	31	1.00	0	1	0	0	2	0	0	0	0	0

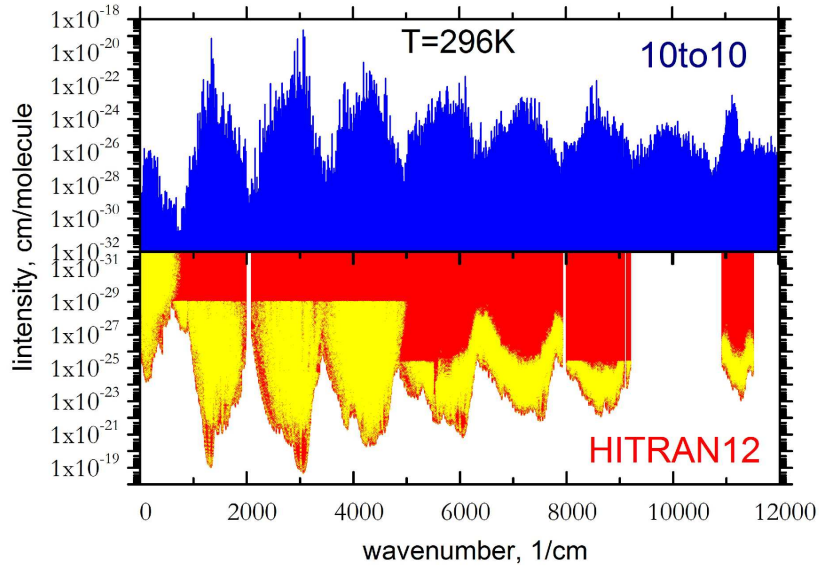
Column	Notation
1	$N$
2	$\tilde{E}$
3	$g_{\text{tot}}$
4	$J$
5	$\Gamma_{\text{tot}}$
6,7,9,12	$n_1 - n_4$
8,10,13	$L_2, L_3, L_4$
11,14	$M_3, M_4$
15	$\Gamma_{\text{vib}}$
16	$J$
17	$K$
18	$\tau_{\text{rot}}$
19	$\Gamma_{\text{rot}}$
20	$N_{J,\Gamma}$
21	$ C_i ^2$
22-30	$v_1 - v_9$

**Table 4.** Extract from the 10to10 Transition file.

$F$	$I$	$A_{IF} / \text{s}^{-1}$
1002348	1180308	1.2167e-04
1033584	1024255	4.5595e-04
10461	27572	1.2159e-03
1046761	1199185	1.5956e-03
1049153	863924	4.4509e-04
1049953	1024823	4.1242e-04
1050761	1024875	7.6355e-05
105546	135097	1.0140e-03
1088309	1292264	2.6590e-06
1099011	1111107	7.0156e-06
1116545	1058555	4.6582e-04
1150480	1236818	1.5768e-04

$I$ : Upper state counting number;  $F$ : Lower state counting number;  $A_{IF}$ : Einstein A coefficient in  $\text{s}^{-1}$ .

**Figure 5.** Absorption of  $^{12}\text{CH}_4$  at  $T = 296$  K: HITRAN 2012 (bottom) Rothman et al. (2013) and 10to10 (top). The yellow stars are to indicate the intensity coverage in HITRAN.



given as circles. Apart from general good agreement between theory and experiment, one can see that the coverage of the experimental  $\text{CH}_4$  data as represented by HITRAN though reasonably good, still has gaps in both the frequency and intensity directions.

Figure 6 gives a number of zoomed-in pictures of several bands, which illustrate the quality of our data. Both the line positions and the absolute intensities agree well with the HITRAN data, at least for the strongest lines. A more detailed line-by-line comparative analysis is planned in the nearest future. Our spectrum seems to disagree with HITRAN 2012 in the wavenumber region  $800\text{--}900\text{ cm}^{-1}$ , where new release of HITRAN has a stronger feature which was not present in the previous, 2008 release of HITRAN (Rothman et al. 2009) or in our calculations. This feature corresponds to two hot, combination bands  $3\nu_4 - 2\nu_2$  and  $3\nu_4 - \nu_3$ . These bands are yet to be characterized experimentally and thus result purely from an extrapolation. We suggest that there is a problem with the effective dipole moment model used to generate these lines. Furthermore, we note that the new HITRAN 2012 lines in the region  $300\text{--}600\text{ cm}^{-1}$  have significantly different (lower) intensities compared to the data in HITRAN 2008 where the latter also agrees well with the 10to10 spectrum.

The intensities of our stick spectrum in the band around the  $7000\text{ cm}^{-1}$  band appear to be very different from those of HITRAN. The bottom-right display of Fig. 6 also shows the spectrum convolved with a  $T = 296$  K Doppler profile, which allows overlapping lines to be added together. This spectrum is in much better agreement with the HITRAN stick intensities, suggesting that most of the intensities given as single lines in HITRAN are actually from blends. Our stick spectrum starts ‘de-focusing’ at  $8000\text{ cm}^{-1}$  in terms of the centre of the bands, this probably indicates the limitations of our refined PES in this region.

**Figure 6.** The absorption spectrum of  $^{12}\text{CH}_4$  at  $T = 296$  K: 10to10 (blue) vs HITRAN 2012 (red) compared for different wavenumber windows. The bottom-right display also shows the 296 K spectrum convolved with the doppler profile (green).

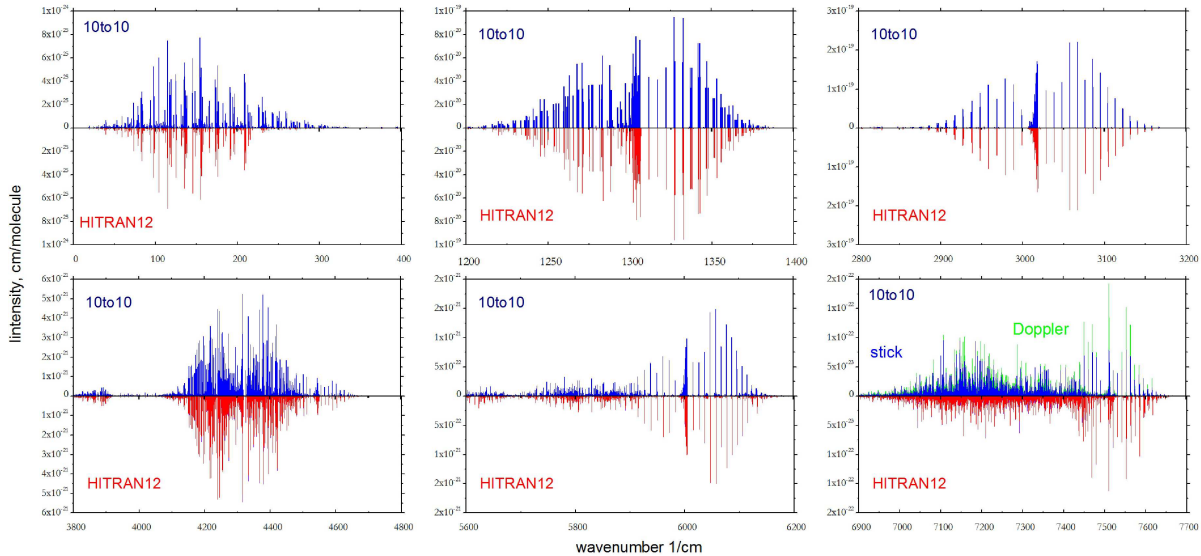


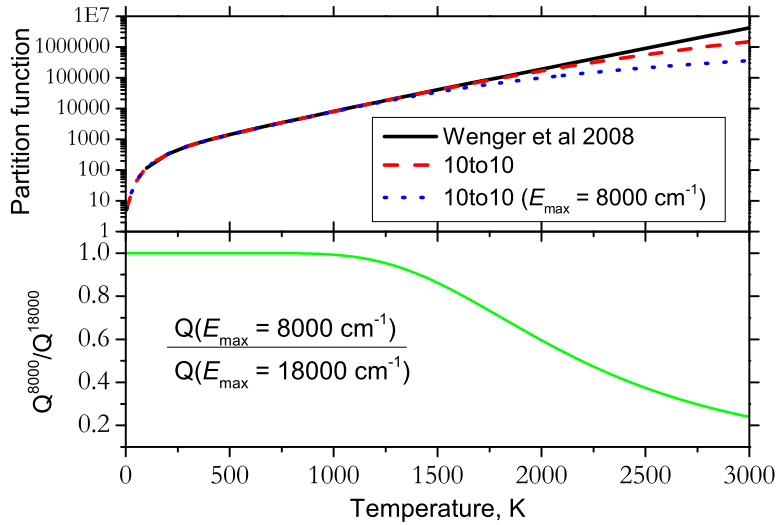
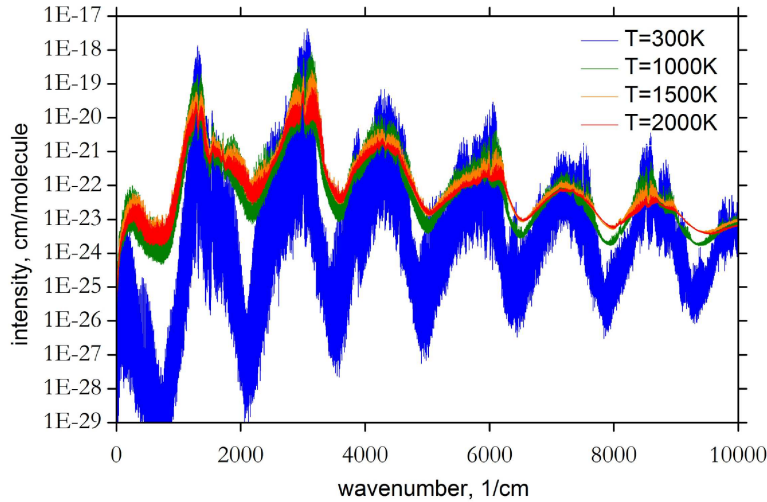
**Table 5.** Summary of available experimental and theoretical methane line lists.

Line list	$T$ , K	wavenumber, $\text{cm}^{-1}$	$N$ lines	$J_{\text{max}}$	$E_{\text{max}}$
Nassar & Bernath (2003)	800, 1000, 1273	2000-6400	16 191, 23 002, 26 821		
Hargreaves et al. (2012)	573, 673, ..., 1673	960-5000	33 955-79 098		
Thi��vin et al. (2008)	1 005, 1 365, 1 485, 1 625	2 700-3 300	4 904, 3 824, 5 647, 2 381, 1 559		
HITRAN 2012		0-11 502	336 830	25	4 263
Warmbier et al. (2009)		0-6 133	1 410 789	34	6 200
MeCaSDa		0-6 446	5 045 392	25	6 340
10to10		0-12 000	9 819 605 160	39	8 000

## 6.2 Hot spectrum of $\text{CH}_4$

### 6.2.1 Experimental comparisons

It is common for the absorption spectra of polyatomic molecules to change dramatically with increased temperature. Figure 8 illustrates the dynamic temperature effect in case of the methane absorption spectrum. Especially the window regions between strong bands gain significant intensity as temperature increases. These window regions are generally under-sampled in laboratory experiments because of their very weak absorption. The corresponding lines compiled mostly from the hot-bands transitions become increasingly important at elevated temperatures when the hot-bands get stronger. The HITRAN-based spectrum significantly underestimates the opacity of  $\text{CH}_4$  in the regions between the strong bands and, as a result, gives the bands the wrong shape. This is especially evident at the higher wavenumbers bands,  $5000\text{--}6000\text{ cm}^{-1}$  and  $7000\text{--}8000\text{ cm}^{-1}$ , where the HITRAN representation of methane is especially sparse. To illustrate the problem of the under-sampling, Table 6 lists opacities (integrated intensities) for the  $H$ ,  $J$  and  $K$  spectral regions (see also below). We used a simple definition of the  $K$  ( $2.0\text{--}2.4\text{ }\mu\text{m}$ ),  $H$  ( $1.5\text{--}1.8\text{ }\mu\text{m}$ ) and  $J$  ( $1.1\text{--}1.4\text{ }\mu\text{m}$ ) regions given also in Table 6.

**Figure 7.** Temperature dependence of the partition function of CH<sub>4</sub>**Figure 8.** Temperature dependence of the absorption cross sections (cm/molecule) of <sup>12</sup>CH<sub>4</sub> computed at  $T = 300, 1000, 1500,$  and  $2000$  K using the 10to10 line list.

Experimentally, the spectrum of hot methane has been the subject of several studies, see Nassar & Bernath (2003) ( $T = 800, 1000,$  and  $1273$  K), Thiévin et al. (2008) ( $T = 1005 - 1820$  K), and Hargreaves et al. (2012) ( $T = 573 - 1673$  K)  $\text{cm}^{-1}$ . Table 5 summarises the coverage of these studies. The 10to10 results given in this table suggest that the absorption by methane in each band is essentially independent of temperature; all previous studies show significantly less absorption by methane at elevated temperatures.

Figure 9 shows the  $T = 1425$  K absorption spectrum of Thiévin et al. (2008) compared to two types of synthetic (10to10) absorption spectra of CH<sub>4</sub> at  $T = 1500$  K: (a) a ‘stick’ spectrum and (b) a Doppler-broadened spectrum. The good agreement with the latter spectrum shows



**Table 6.** Integrated intensities for the  $K$ ,  $H$ , and  $J$  bands from different line lists.

	296 K	1000 K	1200 K	1273 K	1500 K	2000 K
Line list	$K$ band: 4166.7 – 5000.0 $\text{cm}^{-1}$					
Nassar & Bernath (2003)		2.6E-19		1.6E-19		
Hargreaves et al. (2012) <sup>a</sup>		5.2E-19		3.7E-19		
Thiévin et al. (2008)						
HITRAN 2012						
Warmbier et al. (2009)	8.1E-19	1.6E-19	2.0E-19	1.7E-19	9.7E-20	3.0E-20
MeCaSDa	8.1E-19	3.5E-19	4.6E-19	3.8E-19	2.3E-19	7.1E-20
10to10	8.1E-19	2.8E-19	4.0E-19	3.4E-19	2.2E-19	7.6E-20
	7.8E-19	8.0E-19	8.2E-19	8.2E-19	7.8E-19	5.7E-19
	$H$ band: 5555.6 – 6666.7 $\text{cm}^{-1}$					
Nassar & Bernath (2003)				2.3E-20		
Hargreaves et al. (2012)						
Thiévin et al. (2008)						
HITRAN 2012						
Warmbier et al. (2009)	1.0E-19	1.0E-20	1.1E-20	8.9E-21	4.7E-21	1.2E-21
MeCaSDa	2.3E-19	1.5E-20	1.6E-20	1.2E-20	6.3E-21	1.6E-21
10to10	1.3E-19	2.5E-20	3.0E-20	2.4E-20	1.3E-20	3.8E-21
	1.4E-19	1.5E-19	1.6E-19	1.6E-19	1.5E-19	1.1E-19
	$J$ band: 7142.9 – 9090.9 $\text{cm}^{-1}$					
Nassar & Bernath (2003)						
Hargreaves et al. (2012)						
Thiévin et al. (2008)						
HITRAN 2012						
Warmbier et al. (2009)	1.4E-21	7.3E-23			3.0E-23	7.3E-24
MeCaSDa						
10to10	6.0E-20	6.3E-20			6.6E-20	5.2E-20

<sup>a</sup> The actual temperature used by Hargreaves et al. (2012) was  $T = 973$  K.

the importance of the correct description of the line mixing for accurate reconstruction of the line absorption, absent in the experimental line list by Thiévin et al. (2008).

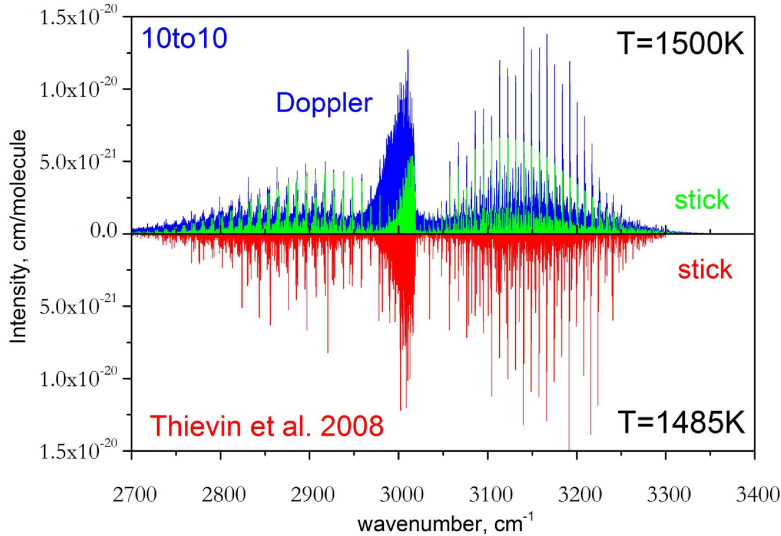
Figure 10 compares the 10to10 absorption (stick) spectrum of  $\text{CH}_4$  at  $T = 1000$  K with the 1000 K absorption spectrum of Nassar & Bernath (2003) and to the  $T = 973$  K spectrum of Hargreaves et al. (2012). We see that there is generally good agreement between theory and experiment. However the integrated absorption intensities are very different, see Table 6. In the region 4166.7 – 5000.0  $\text{cm}^{-1}$  ( $K$ -band) at  $T = 1273$  K the line list of Hargreaves et al. (2012) gives  $I_{\text{tot}} = 3.7 \times 10^{-19}$  cm/molecule, compared to our value,  $8.2 \times 10^{-19}$  cm/molecule. HITRAN 2012 underestimates the opacity at these temperature and region even more, giving  $I_{\text{tot}} = 1.7 \times 10^{-19}$  cm/molecule. For the higher wavenumber regions ( $H$  and  $J$ ) the problem of missing opacities is even more pronounced from one (Nassar & Bernath 2003) to two (HITRAN 2012) orders of magnitude.

A final piece of experimental information are the “PNNL” cross sections provided by Sharpe et al. (2004) ( $\text{cm}^2/\text{molecule}$ ) which are presented at three temperatures,  $T=5$ , 20, and 50 C. Fig. 11 compares the  $T = 50$  C PNNL cross sections with that generated by 10to10.

### 6.2.2 Theoretical comparisons

Warmbier et al. (2009) reported a theoretical hot-line list for methane computed variationally using the program MULTIMODE (Carter & Bowman 1998) in conjunction with an *ab initio* PES and DMS calculated at the RCCSD(T)/aug-cc-pVTZ level of theory. This line list contains 1.4 million lines covering the wavenumbers up to 6200  $\text{cm}^{-1}$  with  $J = 0 \dots 34$  and energies up

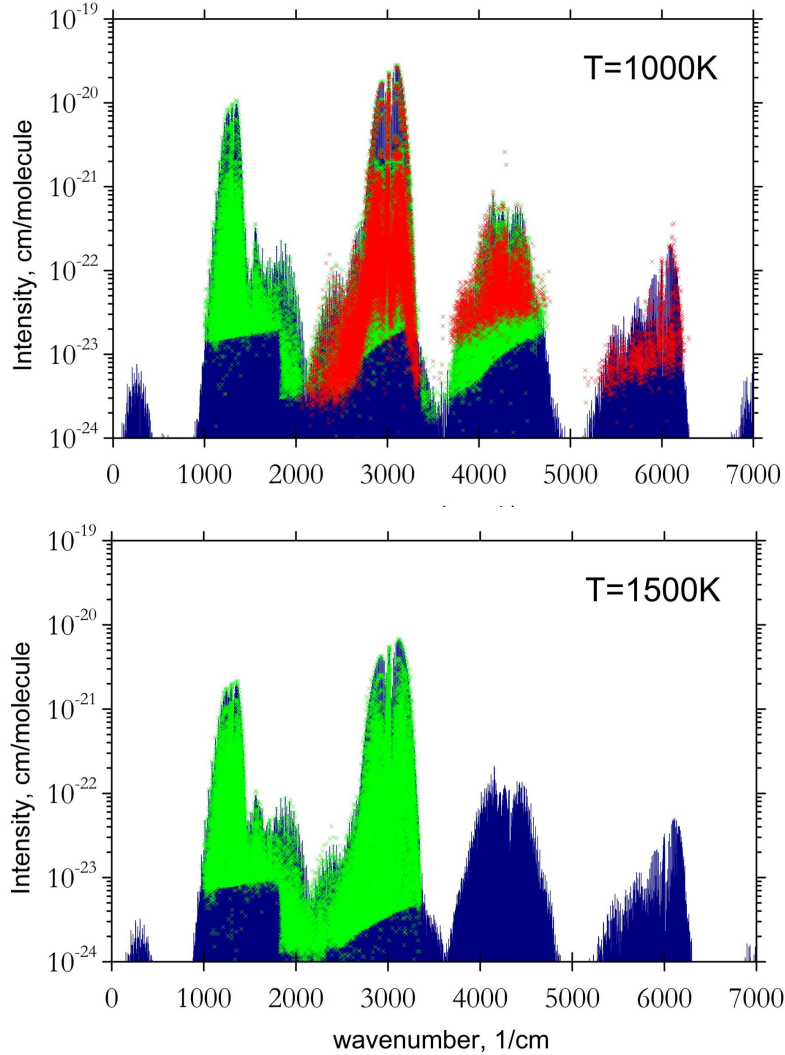
**Figure 9.** The absorption spectrum of  $^{12}\text{CH}_4$  at  $T = 1485$  K. The bottom display shows the experimental intensities (cm/molecule) derived by Thiévin et al. (2008) from their emission spectra in the region  $2700\text{--}3300\text{ cm}^{-1}$ . The top display shows: (sticks) the 10to10 absorption spectrum lines obtained as the maximal intensity at the  $0.2\text{ cm}^{-1}$  wavenumber bin and (Doppler) the 10to10 absorption spectrum convolved with the Doppler profile and integrated over a  $0.1\text{ cm}^{-1}$  wavenumber bin.



to  $6200\text{ cm}^{-1}$  only. We used this line list to generate the cross sections of  $\text{CH}_4$  at  $T = 1500\text{ K}$  assuming Doppler broadening only. Fig. 12 compares these cross sections with those from 10to10 at the same temperature. The significantly lower values of the cross sections by Warmbier et al. (2009) indicate that their line list is very incomplete especially for higher frequencies and for hot bands. The corresponding integrated intensities for the *H* and *K* bands listed in Table 6 give a quantitative illustration of this conclusion. For example, the *H*-band integrated intensity at  $T = 1500\text{ K}$  obtained from the line list of Warmbier et al. (2009) is  $6.3 \times 10^{-21}\text{ cm/molecule}$  which is ten times weaker than the 10to10 value.

Very recently an accurate synthetic line list MeCaSDa was reported by Ba et al. (2013). It was generated using the XTDS software Wenger et al. (2008a). This line list contains 5 045 392 transitions of  $^{12}\text{CH}_4$  with  $J \leq 25$  and covering the wavenumber range up to  $6446\text{ cm}^{-1}$  with lower state energies up to  $6340\text{ cm}^{-1}$ , see Table 5. The line positions are close to experimental accuracy with a reasonable coverage of  $\text{CH}_4$  hot transitions. Figure 12 compares the  $T = 1000\text{ K}$  spectrum generated using MeCaSDa (below  $6446\text{ cm}^{-1}$ ) and that obtained with 10to10. The differences are less pronounced than for HITRAN or Warmbier et al. (2009), however some opacity at high temperature is still missing, see Table 6. For example, for the *H*-band integrated intensity at  $T = 1000\text{ K}$  MeCaSDa gives  $I_{\text{tot}} = 2.5 \times 10^{-20}\text{ cm/molecule}$ , which is 6 times smaller than that of 10to10. At  $T = 1500\text{ K}$  this difference is even more dramatic,  $1.3 \times 10^{-20}$  (MeCaSDa) compared to  $1.5 \times 10^{-19}\text{ cm/molecule}$  (10to10).

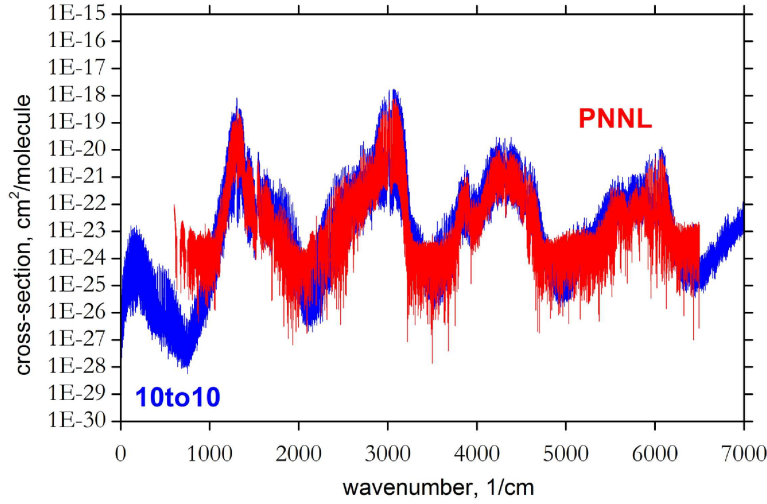
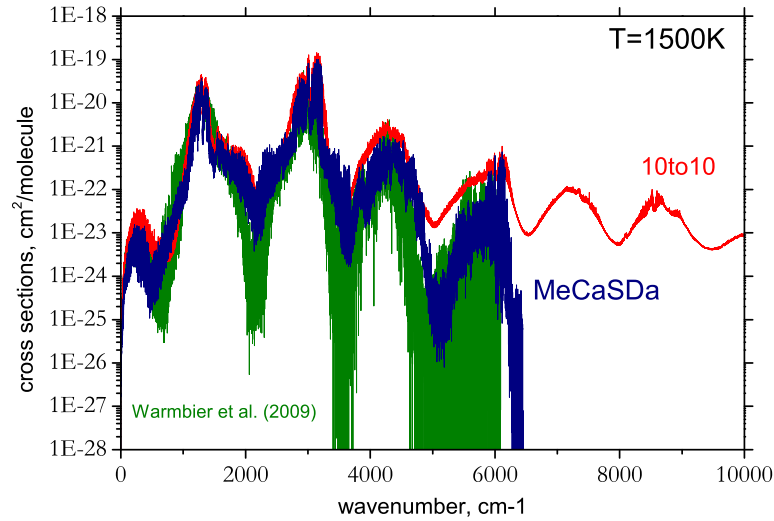
**Figure 10.** Experimental (crosses) and theoretical (blue bars) absorption intensities of  $^{12}\text{CH}_4$  at  $T = 1000$  K and 1500 K. The experimental data are from Nassar & Bernath (2003) (red) and Hargreaves et al. (2012) (green). Note that the actual temperatures used by Hargreaves et al. (2012) were  $T = 973$  K and 1473 K.



### 6.2.3 Astrophysical comparisons

Methane has been detected in the atmospheres of exoplanets, cool stars and comets. We have selected two extra-terrestrial methane spectra recorded at elevated temperatures at relatively high or medium resolution. The several collisions of Comet Shoemaker-Levy 9 with Jupiter was carefully observed in the infrared (Orton et al. 1995). Fig. 13 compares a synthetic 10to10 emission spectrum of methane at  $T = 1400$  K with one of the Jovian spectra recorded during the impact of Comet Shoemaker-Levy 9 on 17 July 1994 Dinelli et al. (1997). Dinelli et al. (1997) identified a number of hot methane features based on the high resolution spectrum of Hilico et al. (1994).

Our other example is associated with the spectroscopy of the methane brown dwarfs. Fig. 14 gives a comparison of a synthetic 10to10 absorption spectrum of  $\text{CH}_4$  at  $T = 1200$  K with the spectrum of the T4.5 brown dwarf 2MASS J0559-1404 centered at  $1.67 \mu\text{m}$  reported by

**Figure 11.** Comparison of the 10to10 and Sharpe et al. (2004) cross sections of  $^{12}\text{CH}_4$  at  $T = 50$  C.**Figure 12.** Theoretical cross sections  $\sigma$  ( $\text{cm}^2/\text{molecule}$ ) of  $^{12}\text{CH}_4$  at  $T = 1500$  K obtained using three line lists: (i) 10to10, (ii) MeCaSDa (Ba et al. 2013), and (iii) Warmbier et al. (2009).

Cushing et al. (2005), who characterised the methane spectral features based on the high resolution  $\text{CH}_4$  spectrum by Nassar & Bernath (2003). In both cases our spectra agree well with the observation and can potentially offer a more complete picture of the methane contributions to the spectral description of cool stars and exoplanets.

## 7 CONCLUSION

We have computed a methane vibration-rotation line list containing almost 10 billion transitions which we call 10to10. The full line list for each of these isotopologues can be downloaded from the CDS, via <ftp://cdsarc.u-strasbg.fr/pub/cats/J/MNRAS/> or <http://cdsarc.u-strasbg.fr/viz-bin/>

**Figure 13.** Jupiter spectrum recorded 17 July 1994 during the impact of Comet Shoemaker-Levy 9 (Dinelli et al. 1997) (red) and 10to10 emission spectrum of CH<sub>4</sub> at  $T = 1400$  K.

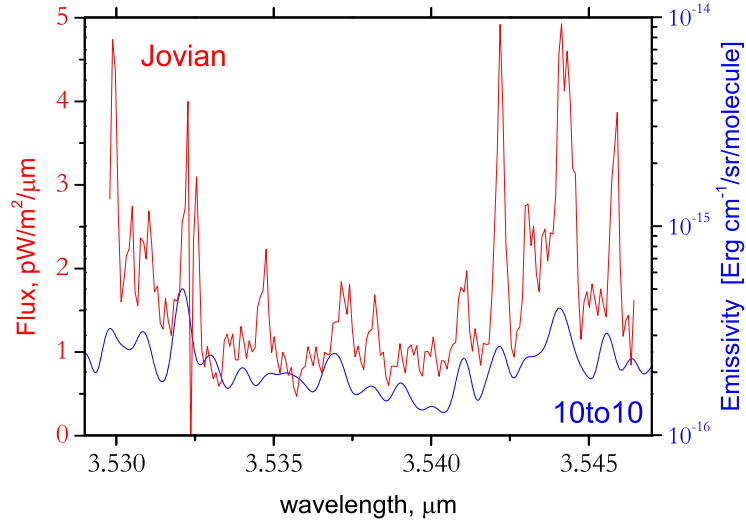
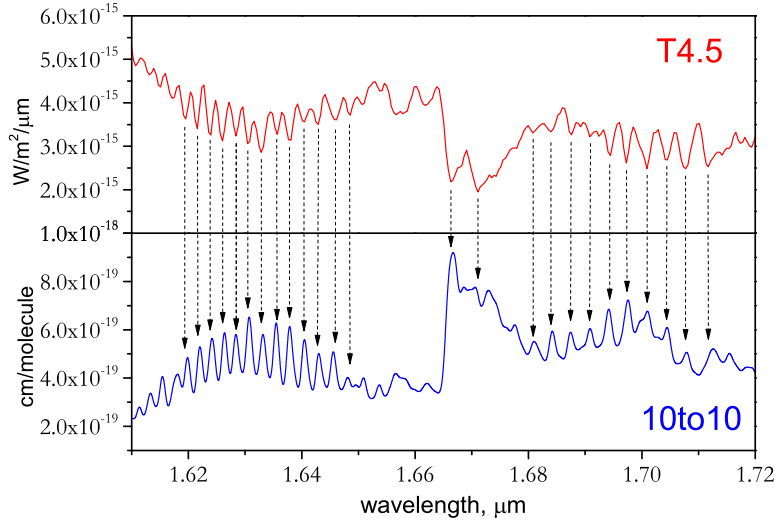


**Figure 14.** The spectrum of the T5 Brown Dwarf 2MASS J0559-1404 (Cushing et al. 2005) compared to the 10to10 absorption spectrum of CH<sub>4</sub> at  $T = 1200$  K. All features are from CH<sub>4</sub>. Arrows are shown to guide the eye.



and from the ExoMol website [www.exomol.com](http://www.exomol.com). The problem with having such an extensive line list is that files are large and difficult to manipulate. The ExoMol project provides facilities for generating cross sections at appropriate temperatures (Hill et al. 2013).

10to10 has been constructed as the next member in the series of line lists provided by the ExoMol project (Tennyson & Yurchenko 2012; Yadin et al. 2012; Barton et al. 2013; J.Barber et al. 2013) which aims to provide comprehensive line lists for studies of hot atmospheres such as exoplanet, brown dwarfs and cool stars. Its construction means that there are now hot line lists for the key set of molecules methane, water (Barber et al. 2006) and ammonia (Yurchenko et al. 2011a). These provide a suitable set of spectroscopic data on hot molecules for systematic mod-

els to be performed on astronomical objects with hot, molecular hydrogen-rich atmospheres. Work in this direction has already started.

However, despite the size of the 10to10 line list it remains incomplete and should only be used with caution for temperatures higher than 1500 K as it will miss a significant proportion of the opacity at these higher temperatures. Furthermore, the effective, empirical character of the underlying potential energy surface and the convergence deficiency of the TROVE nuclear motion calculations means that the accuracy of the energy levels, particularly at higher energies, and hence the related transition frequencies could be improved. Work in this direction will be undertaken in due course.

## ACKNOWLEDGEMENTS

This work was supported by STFC and ERC Advanced Investigator Project 267219. The research made use of the DiRAC@Darwin and DiRAC@COSMOS HPC clusters. DiRAC is the UK HPC facility for particle physics, astrophysics and cosmology and is supported by STFC and BIS. We also thank UCL for use of the Legion High Performance Computer for performing the electronic structure calculations and Bianca Maria Dinelli for providing her cometary data.

## REFERENCES

- Atreya S. K., Mahaffy P. R., Wong A.-S., 2007, *Planet Space Sci.*, 55, 358
- Ba Y. A. et al., 2013, *Journal of Quantitative Spectroscopy and Radiative Transfer*,
- Bailey J., Kedziora-Chudczer L., 2012, *MNRAS*, 419, 1913
- Barber R. J., Tennyson J., Harris G. J., Tolchenov R. N., 2006, *MNRAS*, 368, 1087
- Barton E. J., Yurchenko S. N., Tennyson J., 2013, *MNRAS*, 434, 14691475
- Beaulieu J. P. et al., 2011, *ApJ*, 731, 16
- Bernath P. F., 2009, *Int. Rev. Phys. Chem.*, 28, 681
- Boudon V., Rey M., Loëte M., 2006, *J. Quant. Spectrosc. Radiat. Transf.*, 98, 394
- Brown L. et al., 2013, *Journal of Quantitative Spectroscopy and Radiative Transfer*,
- Bunker P. R., Jensen P., 2004, *Fundamentals of Molecular Symmetry*. IOP Publishing, Bristol
- Campargue A., Leshchishina O., Mondelain D., Kassı S., Coustenis A., 2013, *J. Quant. Spectrosc. Radiat. Transf.*, 118, 49
- Carter S., Bowman J. M., 1998, *J. Chem. Phys.*, 108, 4397
- Cushing M. C., Rayner J. T., Vacca W. D., 2005, *ApJ*, 623, 1115
- Dello Russo N., DiSanti M. A., Magee-Sauer K., Gibb E. L., Mumma M. J., Barber R. J., Tennyson J., 2004, *Icarus*, 168, 186
- Dinelli B. M. et al., 1997, *Icarus*, 126, 107



- Down M. J., Hill C., Yurchenko S. N., Tennyson J., Brown L. R., Kleiner I., 2013, *J. Quant. Spectrosc. Radiat. Transf.*, 130, 260
- Geballe T. R., Kulkarni S. R., Woodward C. E., Sloan G. C., 1996, *ApJ*, 467, L101
- Hargreaves R. J., Beale C. A., Michaux L., Irfan M., Bernath P. F., 2012, *ApJ*, 757, 46
- Hilico J. C., Champion J.-P., Toumi S., Tyuterev V. G., Tashkun S. A., 1994, *J. Mol. Spectrosc.*, 168, 455
- Hill C., Yurchenko S. N., Tennyson J., 2013, *Icarus*, (in press)
- Hougen J., 2001, *Methane Symmetry Operations*. NIST, Gaithersburg, MD., version 1.0 [Online]. Available: <http://physics.nist.gov/Methane>
- Irwin P. G. J., Calcutt S. B., Taylor F. W., Weir A. L., 1996, *J. Geophys. Res.-Planets*, 101, 26137
- J.Barber R., Strange J., Hill C., L.Polyansky O., G.Mellau, Yurchenko S. N., Tennyson J., 2013, *MNRAS*
- Jourdanneau E., Gabard T., Chaussard F., Saint-Loup R., Berger H., Bertseva E., Grisch F., 2007, *J. Mol. Spectrosc.*, 246, 167
- Krasnopolsky V. A., 2012, *Icarus*, 217, 144
- Lucas P. W. et al., 2010, *MNRAS*, 408, L56
- Maillard J.-P. et al., 1995, *Geophys. Res. Lett.*, 22, 1573
- Matyus E., Fabri C., Szidarovszky T., Czako G., Allen W. D., Csaszar A. G., 2010, *J. Chem. Phys.*, 133
- Mielke S. L., Chakraborty A., Truhlar D. G., 2013, *J. Phys. Chem. A*, 117, 7327
- Nassar R., Bernath P., 2003, *J. Quant. Spectrosc. Radiat. Transf.*, 82, 279
- Nikitin A. V., Rey M., Tyuterev V. G., 2011, *Chem. Phys. Lett.*, 501, 179
- Nikitin A. V., Rey M., Tyuterev V. G., 2013, *Chem. Phys. Lett.*, 565, 5
- Orton G., Miller S., Achilleos N., Lam H., Tennyson J., others ., 1995, *Science*, 267, 1277
- Oyanagi C., Yagi K., Taketsugu T., Hirao K., 2006, *J. Chem. Phys.*, 124, 064311
- Rey M., Nikitin A., Tyuterev V. G., 2013a, *Phys. Chem. Chem. Phys.*,
- Rey M., Nikitin A. V., Tyuterev V. G., 2013b, *J. Mol. Spectrosc.*,
- Rhoderick G. C., Dorko W. D., 2004, *Environ. Sci. Technol.*, 38, 2685
- Rothman L. et al., 2013, *J. Quant. Spectrosc. Radiat. Transf.*, 130, 4
- Rothman L. S. et al., 2009, *J. Quant. Spectrosc. Radiat. Transf.*, 110, 533
- Rothman L. S. et al., 2010, *J. Quant. Spectrosc. Radiat. Transf.*, 111, 2139
- Sagan C., Thompson W. R., Carlson R., Gurnett D., Hord C., 1993, *Nature*, 365, 715
- Schwenke D. W., 2002, *Spectra Chimica Acta A*, 58, 849
- Schwenke D. W., Partridge H., 2001, *Spectra Chimica Acta A*, 57, 887
- Sharpe S. W., Johnson T. J., Sams R. L., Chu P. M., Rhoderick G. C., Johnson P. A., 2004, *APPLIED SPECTROSCOPY*, 58, 1452
- Stevenson K. B. et al., 2010, *Nature*, 464, 1161

- Swain M. R. et al., 2010, *Nature*, 463, 637
- Swain M. R., Vasisht G., Tinetti G., 2008, *Nature*, 452, 329
- Tennyson J., 2012, *WIREs Comput. Mol. Sci.*, 2, 698, 10.1002/wcms.94
- Tennyson J., Hill C., Yurchenko S. N., 2013, in *AIP Conference Proceedings*, Vol. 1545, 6<sup>th</sup> international conference on atomic and molecular data and their applications ICAMDATA-2012, AIP, New York, pp. 186–195
- Tennyson J., Yurchenko S. N., 2012, *MNRAS*, 425, 21
- Thiévin J., Georges R., Carles S., Benidar A., Rowe B., Champion J.-P., 2008, *J. Quant. Spectrosc. Radiat. Transf.*, 109, 2027
- Wang X.-G., Carrington, Jr. T., 2013, *J. Chem. Phys.*, 138, 104106
- Warmbier R., Schneider R., Sharma A. R., Braams B. J., Bowman J. M., Hauschildt P. H., 2009, *A&A*, 495, 655
- Wenger C., Boudon V., Rotger M., Sanzharov M., Champion J. P., 2008a, *J. Mol. Spectrosc.*, 251, 102
- Wenger C., Champion J. P., Boudon V., 2008b, *J. Quant. Spectrosc. Radiat. Transf.*, 109, 2697
- Wolff M., Rhein S., Bruhns H., Naehle L., Fischer M., Koeth J., 2013, *Sensors Actuators B Chem.*, 187, 574
- Yadin B., Vaness T., Conti P., Hill C., Yurchenko S. N., Tennyson J., 2012, *MNRAS*, 425, 34
- Yurchenko S. N., Barber R. J., Tennyson J., 2011a, *MNRAS*, 413, 1828
- Yurchenko S. N., Barber R. J., Tennyson J., Thiel W., Jensen P., 2011b, *J. Mol. Spectrosc.*, 268, 123
- Yurchenko S. N., Barber R. J., Yachmenev A., Thiel W., Jensen P., Tennyson J., 2009, *J. Phys. Chem. A*, 113, 11845
- Yurchenko S. N., Tennyson J., Barber R. J., Thiel W., 2013, *J. Mol. Spectrosc.*, 291, 69
- Yurchenko S. N., Thiel W., Jensen P., 2007, *J. Mol. Spectrosc.*, 245, 126

## A APPENDIX: METHANE QUANTUM NUMBERS

Methane is a symmetric five atomic molecule characterised by nine vibrational degrees of freedom with a vanishing permanent dipole moment. It is a very high symmetry molecule of the  $\mathcal{T}_d(M)$  symmetry group. In this work we use the Molecular Symmetry group (Bunker & Jensen 2004) to describe the irreducible representations (irreps) of  $\text{CH}_4$ . Thus the ro-vibrational states of  $\text{CH}_4$  will be assigned with the five irreps,  $A_1$ ,  $A_2$ ,  $E$ ,  $F_1$ , and  $F_2$ , where  $A_1$  and  $A_2$  are one-dimensional (1D),  $E$  is a 2D, and  $F_1$  and  $F_2$  are 3D irreps. Because of the  $i = \frac{1}{2}$  nuclear spins of the hydrogens, the total spin-rotation-vibration states of  $^{12}\text{CH}_4$  is fermionic and degenerate if hyperfine splittings are neglected. This degeneracy gives rise to nuclear statistical weight factors of 5, 5, 2, 3, and 3 for  $\Gamma = A_1, A_2, E, F_1$ , and  $F_2$ , respectively. The symmetry  $\Gamma$  is a

‘good quantum number’ (Bunker & Jensen 2004) as well as the rotational angular momentum quantum number  $J$ , which are two main labels used to classify the ro-vibrational states of  $\text{CH}_4$ . The electric dipole selection rules are given in Eqs. (1) and (2). The dipole moment components of the molecule in the body-fixed frame span the three components of the  $F_2$  irrep,  $F_{2x}$ ,  $F_{2y}$ , and  $F_{2z}$  and the potential energy function is fully symmetric ( $A_1$ ).

Apart from these well-defined, good quantum numbers, like  $J$  and symmetry, it is a common practise in spectroscopy to assign the ro-vibrational states of a molecule using a full set of rotational and vibrational labels which aid characterizing the state in question. These quantum numbers are usually associated with some selected referenced ro-vibrational functions and are used to describe the similarity of the given ro-vibrational eigenfunction to these reference functions. In variational approaches, where the eigenfunction is given as an linear expansion in terms of the basis functions, the similarity can be assessed by identifying the largest contribution to such an expansion (see, for example (Yurchenko et al. 2007)). In this case the basis functions play the role of the reference functions and the labels characterising the corresponding basis functions are used as the approximate quantum numbers for the eigenstate. The standard problem with this, and other approaches, is the strong mixing of basis set functions at high excitations which gives rise to the ambiguity in assignment. Alternatively, the similarity can be established by computing overlaps between the target and reference wavefunctions, see, for example Matyus et al. (2010), where the reference functions can be any functions and are not limited by the choice of the basis set. The conventional choice of the reference functions includes the rigid-rotor functions for the rotation and the normal mode (degenerate) harmonic oscillator eigenfunctions. Even the latter approach suffers from the state mixing problem and thus cannot guarantee unambiguous definition of the quantum numbers.

The difficulty of assigning the methane energy levels is well recognized. Boudon et al. (2006) suggested the following quantum numbers for the vibrational assignment:  $n_i$ ,  $l_i$ ,  $m_i$  and  $C_i$ ,  $i = 3, 4$ , where  $n_i$  is the vibrational quantum number,  $l_i$  is the vibrational angular momentum ( $l_i = n_i, n_i - 2, n_i - 4, \dots, 0$  or  $1$  for  $i = 2, 3, 4$ ),  $C_i$  is a  $\mathcal{T}_d$  irrep and  $m_i$  is multiplicity index for a given set  $(n_i, l_i, C_i)$ . We partly follow this scheme.

We use the largest contribution approach to assign the eigenfunction of methane. Our selection of the quantum numbers for  $\text{CH}_4$  is given in Eq. (3). For the rotation basis, symmetrized rigid-rotor functions  $|J, K, \Gamma_{\text{rot}}\rangle$  are used, where  $K = |k|$ ,  $k$  is the projection of  $\mathbf{J}$  on the body-fixed  $z$ -axis, and  $\Gamma_{\text{rot}}$  is the rotational symmetry. For the vibrations we use nine 1D local (non-normal) mode basis functions  $\phi_{v_i}(\xi_i)$  ( $i = 1, \dots, 9$ ) (see text) which give rise to nine local mode vibrational quantum numbers  $v_i$ . In order to provide the conventional normal mode quantum numbers, our local mode quantum numbers are mapped to their normal mode counterparts by comparing the corresponding symmetry and polyad of basis functions with that of the reference (degenerate) harmonic oscillator functions. The normal mode quantum numbers are  $n_1, n_2, L_2, n_3, L_3, M_3, n_4, L_4, M_4$ . The classification of the normal modes under  $\mathcal{T}_d$  symmetry is

given in Table 1. The quantum numbers  $n_2$  associated with an isotropic 2D harmonic oscillator  $|n_2, l_2\rangle$  ( $E$  symmetry) is complemented with the projection of the vibrational angular momentum  $l_2 = -n_2, -n_2 + 2, \dots, n_2 - 2, n_2$  (Bunker & Jensen 2004). Since the definition of the sign of  $l_2$  is ambiguous (as ambiguous the sign of  $k$ ), we follow the suggestion of Down et al. (2013) and use the absolute value  $L_2 = |l_2| = n_2, n_2 - 2, \dots, 0$  (1) instead. Similarly, the classification of the 3D normal modes 3 and 4 is based on the 3D isotropic harmonic oscillator  $|n_i, l_i\rangle$  (Hougen 2001) ( $i = 3, 4$ ), where  $n_i$  is the vibrational quantum number and  $l_i$  is the vibrational angular momentum. Following the classification by Boudon et al. (2006) we add the multiplicity index  $M_i \leq L_i$  which we associate with the symmetry according with Table 2, where  $M_i$  is odd for  $F_i$  and  $F_2$  and even for  $A_1$ ,  $A_2$ ,  $E$ . Imposing the condition  $M_i \leq L_i$  automatically constrains  $M_i = 0$  as  $A_1$ ,  $M_i = 1$  as  $F_2$ ,  $M_i = 2$  as  $E$ , and  $M_i = 3$  as  $F_2$ . For higher values of  $M_i$  these symmetry designations are repeated as shown in Table 2. We also choose  $M_i = 6 + 12n$  for  $A_2$  and  $M_i = 12n$  for  $A_1$ . It should be noted however that for  $A_1$  and  $A_2$  these variations of  $M_i$  and  $L_i$  produce over-sampled sets and we choose the combinations with smallest  $M_i$ .

Finally, we stress that our stretching vibrational basis set is not based on the harmonic oscillator functions. We use harmonic oscillators only as a reference to correlate the local mode quantum numbers with the conventional normal mode ones.